THE JOURNAL OF BIOLOGICAL CHEMISTRY VOL. 289, NO. 6, pp. 3736–3748, February 7, 2014

Oxidation-induced Structural Changes of Ceruloplasmin Foster NGR Motif Deamidation That Promotes Integrin Binding and Signaling

Received for publication, September 26, 2013, and in revised form, December 11, 2013 Published, JBC Papers in Press, December 23, 2013, DOI 10.1074/jbc.M113.520981

Marco Barbariga[‡1], Flavio Curnis[§1], Andrea Spitaleri[¶‖], Annapaola Andolfo[**], Chiara Zucchelli[¶‖], Massimo Lazzaro[‡], Giuseppe Magnani[‡‡], Giovanna Musco[¶‖], Angelo Corti[§], and Massimo Alessio[‡2]

From the [‡]Proteome Biochemistry, [§]Tumor Biology and Vascular Targeting, [¶]Dulbecco Telethon Institute, [‖]Biomolecular NMR Spectroscopy, [**]Proteomics Service, and [‡‡]INSPE-Institute of Experimental Neurology, San Raffaele Scientific Institute, 20132 Milan, Italy

Background: Asparagine deamidation at Asn-Gly-Arg (NGR) sites leads to the isoAsp-Gly-Arg (isoDGR) integrin-binding motif formation.
Results: Ceruloplasmin (Cp), which contains two NGR sites and is oxidized in cerebrospinal fluid (CSF) in neurodegenerative diseases, can, undergo oxidation-induced structural changes fostering NGR deamidation with gain of integrin binding and signaling properties, *in vitro* and *ex vivo* in pathological CSF.
Conclusion: Cp NGR motifs can deamidate acquiring integrin-binding functions.
Significance: Cp structural changes favor NGR deamidation.

Asparagine deamidation occurs spontaneously in proteins during aging; deamidation of Asn-Gly-Arg (NGR) sites can lead to the formation of isoAsp-Gly-Arg (isoDGR), a motif that can recognize the RGD-binding site of integrins. Ceruloplasmin (Cp), a ferroxidase present in the cerebrospinal fluid (CSF), contains two NGR sites in its sequence: one exposed on the protein surface (^{568}NGR) and the other buried in the tertiary structure (^{962}NGR). Considering that Cp can undergo oxidative modifications in the CSF of neurodegenerative diseases, we investigated the effect of oxidation on the deamidation of both NGR motifs and, consequently, on the acquisition of integrin binding properties. We observed that the exposed ^{568}NGR site can deamidate under conditions mimicking accelerated Asn aging. In contrast, the hidden ^{962}NGR site can deamidate exclusively when aging occurs under oxidative conditions, suggesting that oxidation-induced structural changes foster deamidation at this site. NGR deamidation in Cp was associated with gain of integrin-binding function, intracellular signaling, and cell pro-adhesive activity. Finally, Cp aging in the CSF from Alzheimer disease patients, but not in control CSF, causes Cp deamidation with gain of integrin-binding function, suggesting that this transition might also occur in pathological conditions. In conclusion, both Cp NGR sites can deamidate during aging under oxidative conditions, likely as a consequence of oxidative-induced structural changes, thereby promoting a gain of function in integrin binding, signaling, and cell adhesion.

Asparagine deamidation is a spontaneous chemical reaction that leads to the formation of aspartate and isoaspartate (isoAsp)[3] in proteins. This reaction can occur both *in vitro*, *e.g.*, during protein storage, and *in vivo* during protein aging (1). The rate of Asn deamidation is determined by several factors, including protein sequence and secondary/tertiary structure that, juxtaposing Asn to specific functional groups, can inhibit or accelerate the reaction (1, 2). For example, the presence of a glycine residue following Asn accelerates the deamidation reaction (3). Other elements that affect Asn deamidation are related to the environment like pH, ionic strength, and temperature (1). Asn deamidation has been mostly considered as a protein-damaging reaction because it introduces negative charges into a protein and, in the case of isoAsp formation, causes a change in the peptide backbone length (1). These modifications can alter protein function and stability and render the proteins more susceptible to degradation (1). Therefore, Asn deamidation has been viewed as a sort of molecular timer that marks the spontaneous protein aging (1, 3). *In vivo*, Asn deamidation has been observed to occur in pathological conditions associated with oxidative stress (4–7). For example, in Alzheimer disease (AD), deamidated forms of Tau protein and β-amyloid peptides have been reported to accumulate in characteristic pathological aggregates (6–9).

However, Asn deamidation may also have other potential biological consequences. In fact, it has been shown that the tripeptide Asn-Gly-Arg (NGR) motif can undergo rapid deamidation reactions that result in the formation of isoDGR (isoAsp-Gly-Arg), a motif that can mimic RGD and recognize the RGD-binding site of integrins (10–14). A blast search in a nonredundant *Homo sapiens* database for protein containing NGR sites indicates that ~5% of all proteins contain at least one

[1] Both authors contributed equally to this study.
[2] Supported by Michael J. Fox Foundation for Parkinson's Research Grant 130-012/2310. To whom correspondence should be addressed: Proteome Biochemistry, San Raffaele Scientific Institute, via Olgettina 58, 20132, Milan, Italy. Tel.: 39-2-2643-4725; Fax: 39-2-2643-6585; E-mail: m.alessio@hsr.it.

[3] The abbreviations used are: isoAsp, isoaspartate; Cp, ceruloplasmin; CSF, cerebrospinal fluid; AD, Alzheimer disease; AmBic, ammonium bicarbonate; Cp-ox, oxidized Cp; Cp-AmBic, deamidated Cp; Cp-ox/AmBic, oxidized/deamidated Cp; PIMT, protein L-isoaspartyl methyltransferase; Btp, bathophenanthroline; MD, molecular dynamics.

TABLE 1

Demographic and clinical features of patients and controls

There were no statistical differences among groups based on sex (Fischer's exact test) or based on age (Mann-Whitney test). [C] indicates CSF total protein concentration; there were no statistical differences among groups based on protein concentration (Mann-Whitney test). CN, controls; AD, Alzheimer disease; MMSE, Mini Mental State Examination; M, male; F, female.

	CN			AD			
	Sex	Age	[C]	Sex	Age	[C]	MMSE
			mg/ml			*mg/ml*	
1	M	70	0.37	F	56	0.41	22
2	M	68	0.32	M	75	0.38	18
3	M	71	0.38	M	71	0.39	21
4	M	62	0.16	M	73	0.38	18
5	M	63	0.85	M	72	0.33	7
6	M	54	0.25	F	72	0.41	18
7	F	72	0.40	M	69	0.29	18
8	F	77	0.50	M	64	0.33	18
9	M	61	0.34	F	73	0.45	13
10	M	70	0.28	M	79	0.61	24
11	F	72	0.41	F	78	0.33	21
12	M	79	0.55	F	77	0.33	16
13	M	80	0.40	M	70	0.24	25
14	F	84	0.23	M	77	0.41	27
15	M	81	0.29	F	79	0.53	29
16	M	81	0.39	M	86	0.49	19
	12 M/4 F	71.5 ± 8.53[a]	0.38 ± 0.15[a]	10 M/4 F	73.1 ± 6.84[a]	0.40 ± 0.09[a]	

[a] These values are the means ± S.D.

NGR motif, and ~0.5% contain more than one NGR motif, suggesting a regulated functional role for this motif. Nevertheless, depending on the protein sequences and structures and on environmental conditions, only certain NGR sites with suitable features are likely to undergo deamidation.

The copper protein ceruloplasmin (Cp), a ferroxidase enzyme present in the cerebrospinal fluid (CSF) (15, 16), contains two NGR sites (^{568}NGR and ^{962}NGR). We previously reported that Cp undergoes oxidative modifications in the CSF of Parkinson disease and AD patients (17), as a consequence of changes in the environmental redox status of pathological CSF (18, 19). Cp oxidation causes a decrease in its ferroxidase activity that may have pathological implications (17). Because oxidative conditions might cause structural changes that accelerate Asn deamidation, we investigated whether the Cp NGR motifs can deamidate during aging under oxidative conditions and whether, as a consequence, Cp acquires integrin binding properties mediated by isoDGR.

Here, we show that although both Cp NGR sites can deamidate, the ^{962}NGR motif undergoes deamidation only when Asn aging occurs under oxidative conditions, in which structural changes are induced. The NGR to isoDGR transition in Cp induces gain of integrin binding function, integrin-mediated intracellular signals, and cell pro-adhesive activity. Finally, we show that Cp deamidation is faster in the CSF from AD patients compared with the one from healthy subjects, suggesting that this Cp modification, and the consequent gain of function, might occur *in vivo* in pathological conditions.

EXPERIMENTAL PROCEDURES

Patients

Samples were obtained from the Institute of Experimental Neurology INSPE-Biobank (San Raffaele Scientific Institute, Milan, Italy). After approval from the hospital's ethical committee and informed consent from patients, CSF samples (0.8–1 ml) were collected by lumbar puncture. The analyzed groups were: Alzheimer disease patients ($n = 16$) and healthy controls ($n = 16$) (Table 1). All patients were at first diagnosis and drug-free. Current criteria for the diagnosis of AD (20) were used for patients admission into the study. Exclusion criteria were: HIV or Hepatitis C virus seropositivity; the appearance of other neurodegenerative diseases or previous cerebral ischemic events; and severe metabolic disorders. Control CSF was from patients who underwent lumbar puncture on account of a suspected neurological disease and who proved to be normal and free from pathological alterations after complete CSF analysis and thorough clinico-neuroimaging assessment. Samples were centrifuged (800 × *g*, 10 min at 4 °C) to eliminate cells, then were either immediately processed, or stored at −80 °C in an N_2-supplemented atmosphere to avoid oxidation.

Cell Cultures and Reagents

Human glioblastoma T98G, keratinocyte HaCaT, and endothelial EA.hy926 cell lines (ATCC) were cultured (37 °C in a 5% CO_2 atmosphere) in DMEM (ATCC) supplemented with L-glutamine, and 10% FBS. Human integrins $\alpha5\beta1$, $\alpha v\beta3$, and $\alpha v\beta5$ (Immunological Sciences), recombinant $\alpha v\beta6$ and $\alpha v\beta8$ (R&D System), and human plasma purified Cp (Alexis Biochemicals) were used.

Oxidation and Asparagine Accelerated Aging Treatments

Oxidation and accelerated Asn aging treatments were performed by incubating purified Cp at 37 °C in various buffers as described below. Oxidized Cp was prepared as follows: purified Cp was diluted at 1 mg/ml in PBS buffer containing in 10 mM H_2O_2 solution and incubated for 16 h at 37 °C. Deamidated Cp was prepared as follows: purified Cp was diluted 1 mg/ml in 100 mM ammonium bicarbonate (AmBic) buffer, pH 8.5, incubated for 16 h at 37 °C, and stored at −20 °C until analysis. This condition is known to favor Asn deamidation at the NGR site (10). Before use in the assays, Cp was dialyzed against PBS using Slide-A-lyzer dialysis cassette 10,000 molecular weight cutoff (Pierce). Oxidized and deamidated Cp was obtained by combining the above treatments. These products are hereinafter

referred to as "oxidized Cp" (Cp-ox), "deamidated Cp" (Cp-AmBic), and "oxidized/deamidated Cp" (Cp-ox/AmBic), respectively. Aging of Cp in CSF was performed by adding purified Cp (final concentration, 20 μg/ml) to CSF either from healthy subjects or from AD patients. CSF samples were then left to incubate for different time (0, 3, 6, 9, and 12 days) at 37 °C under nitrogen conditioned atmosphere, to avoid the exposure to atmospheric oxidative environment.

Binding of Cp to Integrins and Competition with isoDGR Peptide

$\alpha5\beta1$, $\alpha v\beta3$, $\alpha v\beta5$, $\alpha v\beta6$, and $\alpha v\beta8$ integrins (1 μg/ml in PBS with Ca^{2+}/Mg^{2+}; DPBS, Cambrex) were added to 96-well polyvinylchloride plates (BD Biosciences) and incubated 12 h at 4 °C. Subsequent steps were carried out at 20 °C. After blocking (3% BSA-PBS), the plates were filled with: Cp solutions (2–20 μg/ml in binding buffer: 25 mM Tris-HCl, pH 7.4, 150 mM NaCl, 1 mM $MgCl_2$, 1 mM $MnCl_2$, 0,05% Tween, 1% BSA) or CSF samples from healthy subjects or AD patients supplemented with Cp (prepared as described above, diluted in binding buffer) and incubated for 2 h. Binding was detected using a polyclonal anti-human Cp Ab (Abcam ab8813) followed by a secondary HRP conjugate Ab (Abcam) and by *o*-phenylendiamine chromogenic substrate. Competitive binding assays were performed by mixing 10 μg/ml of either the acetyl-CisoDGRCGVRSSSRTPSDKY peptide (isoDGR peptide) or the control peptide CARACGVRSSSRTPSDKY (ARA peptide) (12) with Cp-ox/AmBic solutions (20 μg/ml) and mixing isoDGR peptide (30 μg/ml) with CSF samples spiked with Cp (20 μg/ml). The mixtures were added to microtiter plates coated with integrin, and the binding assay was carried out as described above. Cp bound to the $\alpha v\beta6$-coated plates was analyzed as follow; after the binding, the plates were washed and incubated with Laemmli buffer (5 min at 100 °C) to promote protein detachment, the solution was then collected and subjected to SDS-PAGE and Western blot analyses as described (17) using a polyclonal anti-human Cp Ab (Abcam). Images were acquired using a laser densitometer (Molecular Dynamics).

Cell Adhesion Assay and Protein L-Isoaspartyl Methyltransferase (PIMT) Treatment

96-well polyvinyl chloride microtiter plates were coated with either untreated or treated Cp or with Cp that was immunoprecipitated (see below) after aging in healthy or AD CSF (1–20 μg/ml in 50 mM Na_3PO_4, pH 7.3, 150 mM NaCl, 16 h at 4 °C). After washing and blocking with 3% BSA-DPBS, the plates were seeded with HaCaT, EA.hy926, and T98G cells diluted in 0.1% BSA-DMEM (40,000 cells/well) and left to adhere for 3 h at 37 °C. Adherent cells were fixed and stained with crystal violet as described (14), and adhesion was evaluated as adsorbance at 570 nm. For each treatment condition, cell spreading was evaluated comparing cell area in different microscopy fields. To measure cell area, pixels were automatically detected by image software analysis (Progenesis PG240; Nonlinear Dynamics). For PIMT treatment, plates coated as described above, were washed and filled with 45 μl of 0.02 mM *S*-adenosyl-L-methionine in 50 mM Na_3PO_4, pH 6.8, and 5 μl of PIMT solution (from IsoQuant isoaspartate detection kit; Promega) and incubated at 37 °C for 16 h. Then plates were washed, and cell adhesion assay was performed as described above.

Cp Immunoprecipitation from CSF

After incubation in healthy or AD CSF, spiked purified Cp was immunoprecipitated using protein G-agarose beads (Invitrogen) coated with an anti-Cp antibody (Abcam ab8813). The antibodies were cross-linked to the beads with 20 mM dimethyl pimelimidate (Sigma) and added to the CSF supplemented with Cp; the solution was then incubated for 24 h at 4 °C under gentle stirring. Beads were washed, and Cp was eluted with 0.1 M glycin solution, pH 2.5; samples were immediately diafiltered with PBS using an Amicon filter device.

Bathophenanthroline Assay

Ferroxidase activity of Cp after aging in CSF was evaluated on immunoprecipitated Cp by bathophenanthroline (Btp) assay as in Ref. 17. Briefly, immunoprecipitated Cp (1.25 μg) was incubated with 80 mM $FeSO_4$ (ferrous form) and analyzed after 1 h with a solution of 1 mM Btp in acetate buffer, pH 6.2. A decrease in Btp-Fe^{2+} complex absorbance at 535 nm derives from ferrous iron oxidation into ferric form (Fe^{3+}).

Mass Spectrometry Analysis

Samples were dialyzed against digestion buffer and incubated 2 h at 20 °C with trypsin (10 ng/μl; Roche Applied Science). Digested samples were desalted (Stage tips C18; ThermoScientific) and injected in a capillary chromatographic system (EasyLC; Proxeon Biosystem). Peptide separations occurred on a 25-cm reverse phase silica capillary column, packed with 3-μm ReproSil 100 Å C18 AQ. A gradient of acetonitrile eluents was used to achieve separation (flow rate, 0.15 μl/min). MS analysis was performed by nanoLC-MS/MS using an LTQ-Orbitrap (ThermoScientific) equipped with a nanoelectrospray ion source (Proxeon Biosystems). Full scan spectra were acquired with the lock mass option, resolution set to 60,000, and mass range from m/z 350 to 1700 Da. The six most intense doubly and triply charged ions were selected and fragmented in the ion trap. All MS/MS samples were analyzed using Mascot (v.2.2.07; Matrix Science) and X!Tandem (within Scaffold software, v.2_06_00, 2007; Proteome Software Inc.) search engines to search the UniProt_Human Complete Proteome_cp_hum_2012_07. Searches were performed with three missed cleavages allowed, N terminus acetylation, methionine oxidation, and deamidation of asparagine/glutamine as variable modifications. Mass tolerance was set to 5 ppm and 0.6 Da for precursor and fragment ions, respectively. Scaffold was used to validate MS/MS-based peptide and protein identifications. Protein thresholds were set to 99.0% and two peptides minimum, whereas peptide thresholds were set to 95% minimum.

Circular Dichroism and Melting Curves

CD spectra were acquired for Cp and Cp after oxidative and aging treatments (at 1 μM in 50 mM PBS, pH 7) on a Jasco J-815 CD spectrometer at 20 °C. Each spectrum was averaged using four accumulations collected in 0.1-nm intervals with an average time of 0.5 s. The protein spectra were corrected by sub-

tracting the corresponding buffer spectra and then smoothed. The observed ellipticity (mdeg) was converted into molar residue ellipticity [θ] (deg cm^2 dmol^{-1}). Melting curves were calculated recording CD spectra in continuous from 20 to 96 °C (1 °C intervals) in a wavelength range from 190 to 260 nm to achieve the better resolution. Melting temperature (T_m) was calculated by nonlinear fitting Boltzmann sigmoidal with Prism V4.03 software (GraphPad Inc.).

Molecular Dynamics Simulations and Docking Calculations

Homology Modeling—I-TASSER server was used to predict the secondary and tertiary structure of $\alpha v\beta 6$ integrin (21).

Molecular Dynamics (MD) Simulations—MD simulations were performed on Cp wild type (P00450; Protein Data Bank code 2J5W), using the GROMACS 4.5.4 package (22) with the optimized parameters for liquid simulation force field. The ^{568}isoDGR-Cp and $\alpha v\beta 6$ systems have been simulated in the same manner. Three independent 50-ns-long MD simulations (150-ns production run) were performed for Cp to allow for better conformational sampling, whereas three independent 10-ns-long MD simulations (30 ns) were performed for $\alpha v\beta 6$ to get a set of structures to be used in docking calculations. All the analysis were performed using the GROMACS utilities on the last 40 ns of each simulation concatenated in a single trajectory (120 ns total). In particular, cluster analysis were performed using the Gromos algorithm.

Docking Calculations—Docking calculations of ^{568}isoDGR-Cp on the globular head of the extracellular part of $\alpha v\beta 6$ have been performed using the docking program HADDOCK2.0 (23) with the optimized parameters for liquid simulation force field. We have docked a bundle of 27 ^{568}isoDGR-Cp structures onto a bundle of 10 $\alpha v\beta 6$ structures, which correspond to the centers of the clusters obtained from MD simulations. The protocol follows a three-stage docking procedure: (*a*) randomization of orientations and rigid body minimization, (*b*) simulated annealing in torsion angle space, and (*c*) refinement in Cartesian space with explicit water. Ambiguous interaction restraints ($\alpha v\beta 6$: residues 150, 218, 506, 547, 548, 601, and 815; ^{568}isoDGR-Cp: residues 568–570) were derived from the known interactions of the isoDGR motif of the cyclic peptide with $\alpha v\beta 6$ (11). The best 200 solutions in terms of intermolecular energies were selected for a semiflexible simulated annealing in which the side chains of $\alpha v\beta 6$ and of the ^{568}isoDGR-Cp located at the binding interface were allowed to move in a semirigid body docking protocol to search for conformational rearrangements. The models were then subjected to a water refinement step. The single best docked solutions were analyzed according to hydrogen bonds, salt bridge contact, and buried surface accessibility.

Statistical Analysis

Categorical data were analyzed by using Fisher's exact test and two-tailed p value. Continuous data were evaluated by unpaired Student's t test, if the data passed the normality test for Gaussian distribution as assessed by the Kolmogorov-Smirnov test or were evaluated by Mann Whitney test; a two-tailed p value was used for the comparison of two means and standard error. In all analyses, $p < 0.05$ was considered to be statistically significant. The analysis was performed with Prism V4.03 software (GraphPad Inc.).

Reverse Phase Protein Array Analysis

HaCaT cells were incubated (30 or 120 min) with either Cp or aged/oxidized Cp. Cell lysates obtained with Zeptosens CLB1^{TM} lysis buffer (Bayer) were spotted on arrays and analyzed using Zeptosens custom service (Bayer). A set of 40 Abs, specific either for protein expression or for residue phosphorylation, that identify 25 pairs of phosphorylation rate for 16 different proteins belonging to the integrin signaling pathway (Kyoto Encyclopedia of Genes and Genomes; ko04510 and ko04810) were reacted in a standard Zeptosens profiling assay. Mean referenced fluorescence intensity (RFI) obtained from Ab reactivity were used to evaluate the proportion of specific residues phosphorylation (RFI − (phos-protein-x)/RFI − (protein-x)) for each protein. Then the phosphorylation proportion of the cell treated with aged/oxidized Cp was compared with that of the time-related control Cp (Cp-ox/Cp, 30 min; Cp-ox/Cp, 120 min) to define whether the phosphorylation rate was unaffected (value = 1), induced (value > 1), or inhibited (value < 1) by Cp-ox. Phosphorylation rate was analyzed by hierarchical clustering performed with Mev4.6 v10.2 software (24); the 25 data series of protein phosphorylation rate in the two different conditions (Cp-ox/Cp, 30 min; Cp-ox/Cp, 120 min) were clustered into groups on the basis of the distances between the data series reported as covariance correlation.

RESULTS

Accelerated Aging of Cp under Oxidative Conditions Causes Deamidation of NGR Sites—Sequence analysis of purified Cp by tandem MS showed that both ^{568}NGR and ^{962}NGR motifs were not deamidated (Fig. 1*A* and *B*, untreated) and that protein oxidation by incubation in 10 mM H_2O_2 at 37 °C cannot convert NGR to DGR/isoDGR (Fig. 1*A* and *B*, ox). In contrast, protein incubation in 100 mM AmBic or AmBic plus 10 mM H_2O_2, *i.e.*, solutions that respectively mimic accelerated asparagine aging conditions (AmBic) (10) and accelerated asparagine aging under oxidative conditions (ox/AmBic), the ^{568}NGR motif was partially deamidated (Fig. 1*A*). Interestingly, the ^{962}NGR motif was partially deamidated exclusively following Cp aging under oxidative conditions (Fig. 1*B* ox/AmBic). The presence of Asp in place of Asn in the AmBic-treated Cp indicates that a deamidation reaction occurred at the two NGR sites of Cp, although MS did not ascertain whether DGR or isoDGR isoform was present.

A possible explanation for the different behavior of the ^{568}NGR and ^{962}NGR motifs may arise from analysis of the crystallographic Cp structure (Protein Data Bank code 2J5W) (25), which reveals that the ^{568}NGR motif is exposed on the surface of the protein, whereas the ^{962}NGR motif is less exposed and therefore less accessible to the solvent (Fig. 2*A* and *B*). The two sequences display differing tertiary contexts (Fig. 2*C* and *D*) that might in turn influence deamidation rates differentially. We then attempted to clarify the structural differences between the two sequences by a computational approach. Molecular dynamics simulations on wild type Cp (Protein Data Bank code 2J5W) showed a relatively stable structure with large fluctua-

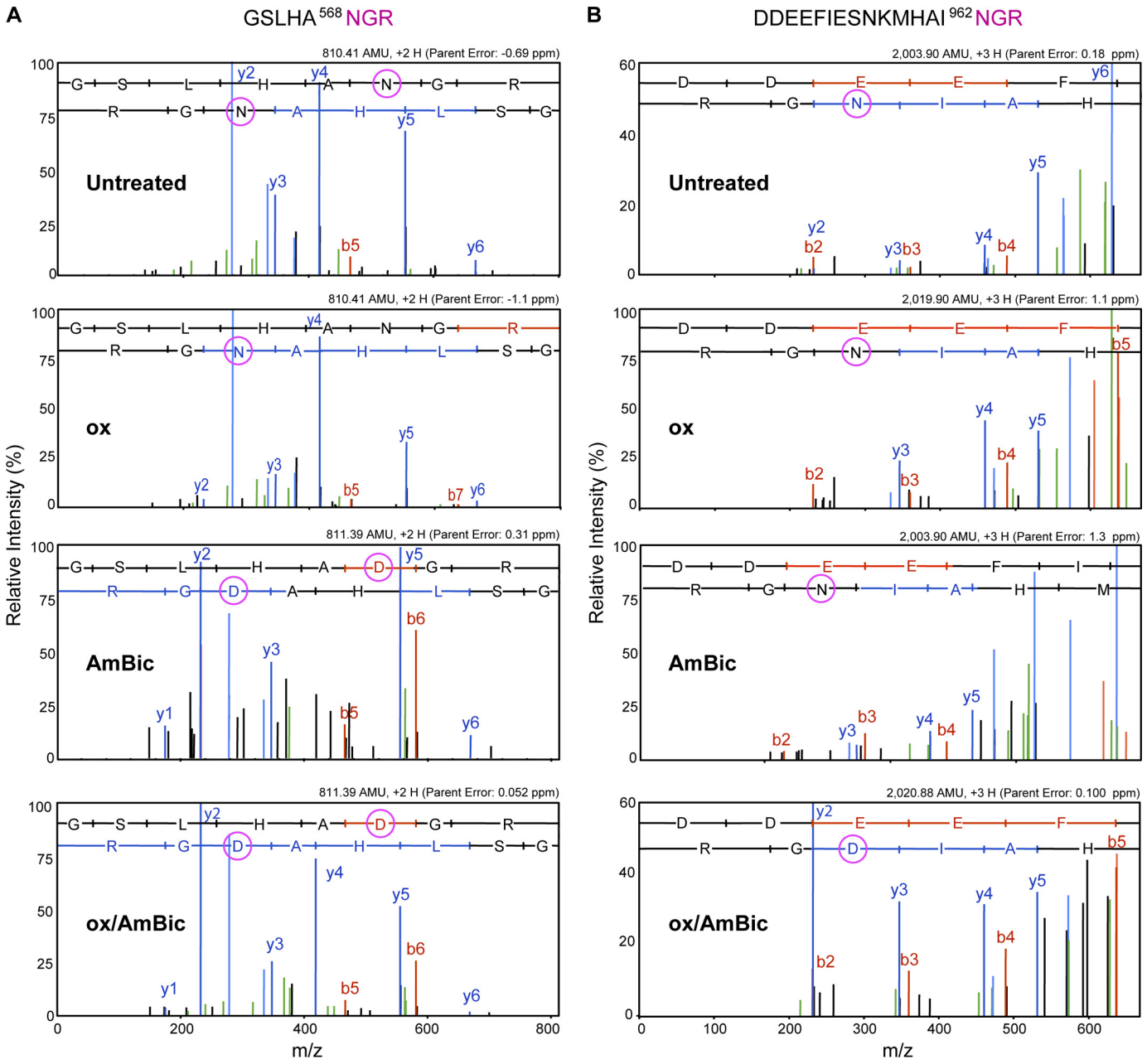

FIGURE 1. **Mass spectrometry analysis shows that the NGR motifs are deamidated during Cp aging under oxidative conditions.** *A*, zoomed annotated ESI-MS/MS spectra of the peptide 563–570 derived from trypsin digestion of Cp upon different treatments: *Untreated*, resting conditions; *ox*, oxidation by Cp incubation in the presence of H_2O_2; *AmBic*, accelerated Asn aging by Cp incubation in the presence of ammonium bicarbonate buffer; *ox/AmBic*, mimicking accelerated Asn aging under oxidative conditions by Cp incubation in the presence of AmBic and H_2O_2. *B*, zoomed annotated ESI-MS/MS spectra of the peptide 948–964 derived from trypsin digestion of Cp upon different treatments as in *A*. Only principal fragmentation series (*b* and *y*) are indicated. The molecular weight, the charge state, and the error of the peptides are reported. Deamidation was inferred by sequencing the D amino acid corresponding to $N + 1$ Da increased molecular mass.

tions of loop regions (Fig. 2*E*). Notably, the root mean square fluctuations, as calculated throughout the simulation, suggest that the two NGR sequences are more rigid than the other residues (Fig. 2*F*). Importantly, the ^{568}NGR sequence is steadily accessible to the solvent throughout the simulation, whereas ^{962}NGR is buried inside the protein and is blocked in a stable conformation by polar interactions with neighboring amino acids (Fig. 2*C* and *D*). Accordingly, we hypothesized that oxidation might affect the Cp structure and promote the exposure of the ^{962}NGR motif, which in turn adopts a favorable conformation for deamidation. Indeed, it has been previously inferred that Cp structure is affected by oxidation (17, 26–28).

Cp Oxidation Induces Secondary Structure Changes—CD spectra obtained for purified Cp indicated that the secondary structure of Cp, which is principally composed of β-strands (45.5%, as evaluated by Uniprot tool), was partially affected by Cp-AmBic treatment (Fig. 2*G*, *black line versus blue line*); notably, large spectra changes occurred upon Cp-ox and -ox/AmBic treatment, suggesting structural alterations (Fig. 2*G*, *black line versus green* and *orange lines*). Interestingly, the spectra profile

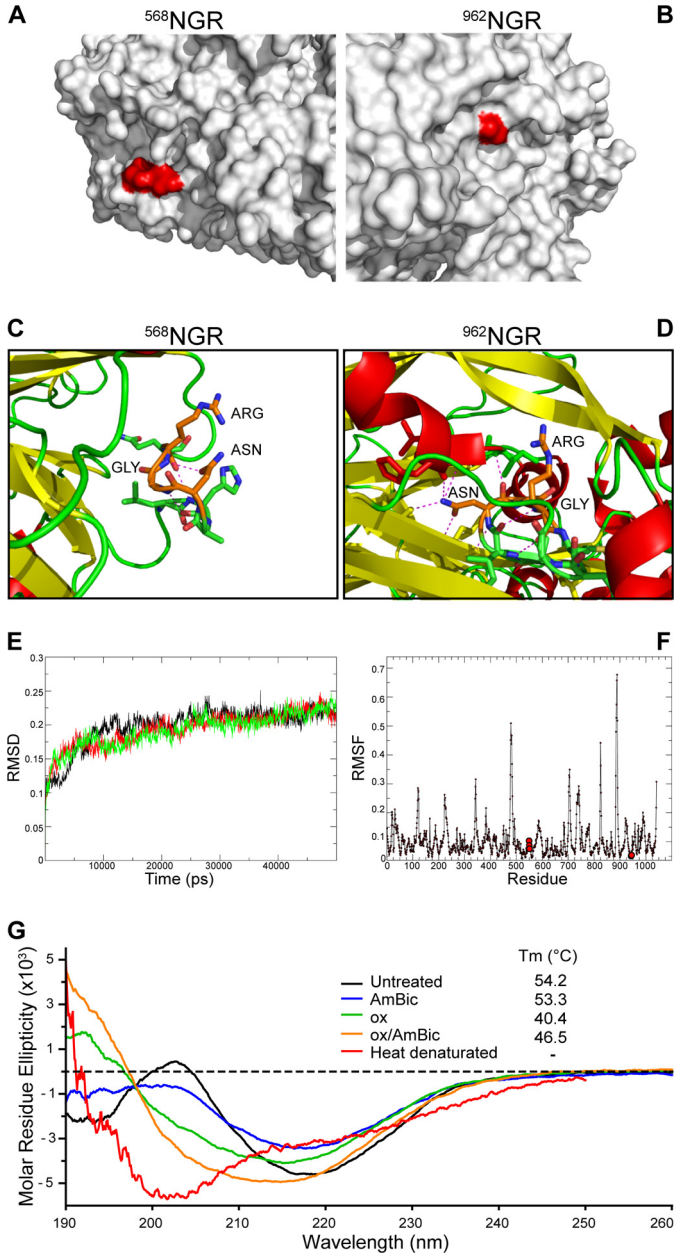

FIGURE 2. **NGR motifs structural analysis, Cp molecular dynamics modeling, and circular dichroism analysis indicate that ^{962}NGR is buried inside Cp structure and that secondary structure changes induced by oxidative conditions might allow its surface exposure.** *A* and *B*, surface representation of Cp. In *red* are highlighted the ^{568}NGR and ^{962}NGR sequences, respectively, as calculated by the GROMACS g_sas tool on crystallographic Cp structure (Protein Data Bank code 2J5W). The higher solvent-accessible surface of ^{568}NGR is represented by the larger size of the *red-colored region*. *C* and *D*, cartoon representation of ^{568}NGR and ^{962}NGR sequences in Cp. The NGR amino acids are shown as *orange sticks*. The hydrogen bonds are shown as *red dashed lines*. ^{568}NGR is engaged in short range polar interactions between GLY and ASN, whereas ^{962}NGR sequence is mostly involved in strong interactions with the rest of the protein. *E*, Cα root mean square deviations from the initial Cp structure. The three different trajectories calculated by molecular dynamics modeling, shown in *red*, *black*, and *green*, respectively, indicate a relatively stable structure. *F*, Cα root mean square fluctuations of the concatenated molecular dynamics simulations (3 $\times$ 50 ns, 150-ns total simulation time). ^{568}NGR and ^{962}NGR are indicated with *red circles*. The plot shows large fluctuations localized in the loop regions, notably the two NGR sequences show a rigid behavior, with low root mean square fluctuation values along the whole simulation. *G*, circular dichroism spectra of Cp after different treatments: resting conditions (*Untreated*, *black line*), accelerated Asn aging (*AmBic*, *blue line*), oxidation (*ox*, *green line*), accelerated Asn aging under oxidative conditions (*ox/AmBic*, *orange line*), and heat denaturation (*red line*). Each spectrum was averaged using four accumulations collected in 0.1-nm wavelength intervals with an average time of 0.5 s. The observed ellipticity (mdeg) was converted into molar residue ellipticity [θ] (deg cm^2 dmol^{-1}). For each treatment, the melting temperature (T_m) is also indicated.

obtained with heat-denatured Cp (Fig. 2*G*, *red line*), which showed a pronounced minimum toward random coil structure (~200 nm), differed from that of Cp obtained in -ox/AmBic conditions. These data suggest that Cp oxidation or accelerated Asn deamidation under oxidative conditions induces secondary structure changes but does not unfold the protein. Comparison of the protein melting temperatures (T_m) before and after the different treatments shows that oxidation induces the strongest destabilizing effect, as assessed by the decreased T_m after oxidation (Cp, 54.2 °C; Cp-ox/AmBic, 46.5 °C; Cp-ox, 40.4 °C); in contrast, the AmBic treatment did not change the Cp thermostability (Cp-AmBic, 53.3 °C)(Fig. 2*G*).

Cp Aged under Oxidative Conditions Binds Integrins—We investigated whether Cp Asn accelerated aging under oxidative conditions, *i.e.*, the condition that may occur in some neurodegenerative diseases, can induce integrin binding via isoDGR formation. *In vitro* binding assays to purified integrins showed negligible binding of untreated Cp, whereas after accelerated Asn aging in AmBic alone or in the presence of oxidative conditions (-ox/AmBic), Cp acquired clear binding properties to $\alpha v\beta 5$, $\alpha v\beta 6$, $\alpha v\beta 3$, and $\alpha v\beta 8$, albeit to differing degrees (Fig. 3*A*). Of note, oxidation alone was ineffective (not shown). Based on the observed additional increase of binding of Cp aged under oxidative conditions to $\alpha v\beta 6$ compared with Cp aged alone, and with the $\alpha v\beta 6$ integrin expressed by epithelial cells, this integrin was used for further analysis. Interestingly, the -ox/AmBic treatment increased the binding to $\alpha v\beta 6$ (Fig. 3*A*) in a dose-dependent manner (Fig. 3*B*). Competitive binding experiments, performed either with the isoDGR peptide capable to bind the RGD binding pocket of integrins (12) or with the control ARA peptide, showed that the isoDGR peptide could abolish the binding of oxidized-aged Cp to the $\alpha v\beta 6$ integrin (Student's *t* test, $p < 0.0001$) (Fig. 3*C*), supporting the role of Cp NGR deamidation in the acquisition of binding activity after aging. The effect of Cp accelerated aging under oxidative conditions was also investigated by Western blot analysis. Untreated Cp showed a principal band of 150 kDa, as expected for a full-length protein (Fig. 3*D*), whereas the treatment caused the appearance of an additional band at >250 kDa. These data suggest that the treatment generating reactive succinimide intermediates on Cp may cause intermolecular aggregation, likely caused by reaction with the amino group present in neighbor Cp molecules (29). Remarkably, both products, full-length Cp and aggregates, bind $\alpha v\beta 6$ integrin (Fig. 3*D*). Taken together, these results indicate that accelerated Asn aging under oxidative conditions promotes the Cp ability to bind integrin RGD-binding pockets, presumably via NGR to isoDGR conversion.

Molecular Dynamics Simulations and Docking Calculations Indicate That ^{568}isoDGR-Cp Can Interact with $\alpha v\beta 6$ Integrin—Our results indicated that the accelerated Asn aging under oxidative conditions leads to the deamidation of both ^{568}NGR and ^{962}NGR motifs in the Cp sequence. Computational approaches have been exploited to evaluate the possibility for deamidated

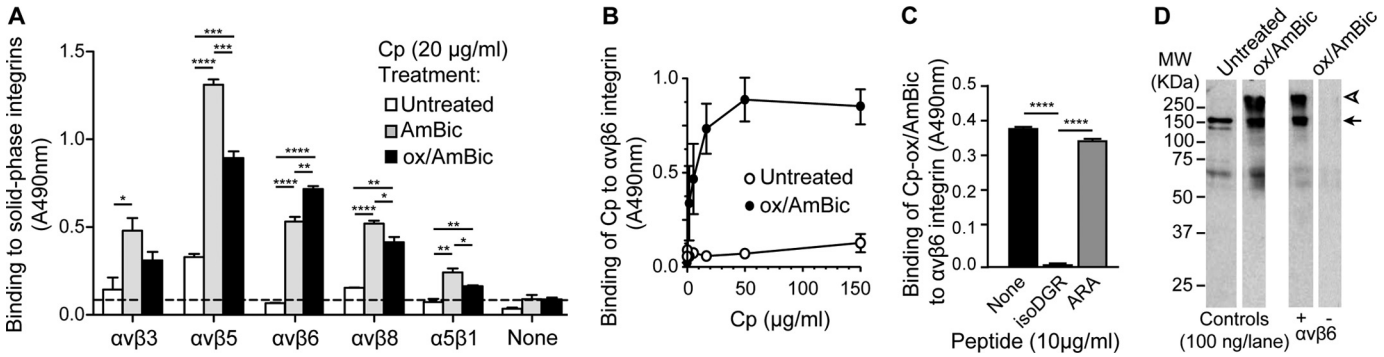

FIGURE 3. **Cp aged under oxidative conditions is able to bind integrins via isoDGR motifs.** *A*, screening by ELISA of the binding to several integrins of Cp under resting conditions (*Untreated*), after Asn accelerated aging (*AmBic*), or after Asn accelerated aging under oxidative conditions (*ox/AmBic*). *B*, analysis of the dose-dependent binding to αvβ6 of untreated Cp or aged/oxidized Cp (*ox/AmBic*). *C*, competitive binding of aged/oxidized Cp (*Cp-ox/AmBic*) to αvβ6 with the isoDGR peptide and control ARA peptide. *D*, Western blot analysis of the Cp-ox/AmBic compared with the untreated Cp (*Controls*) and of the Cp-ox/AmBic eluted from the ELISA microplate either coated (+) or noncoated (−) with αvβ6. All the assays were performed in triplicate for three independent experiments ($n = 3$). Statistical significance reported as p values was evaluated by Student's t test. ****, $p < 0.0001$; ***, $p < 0.001$; **, $p < 0.01$; *, $p < 0.05$.

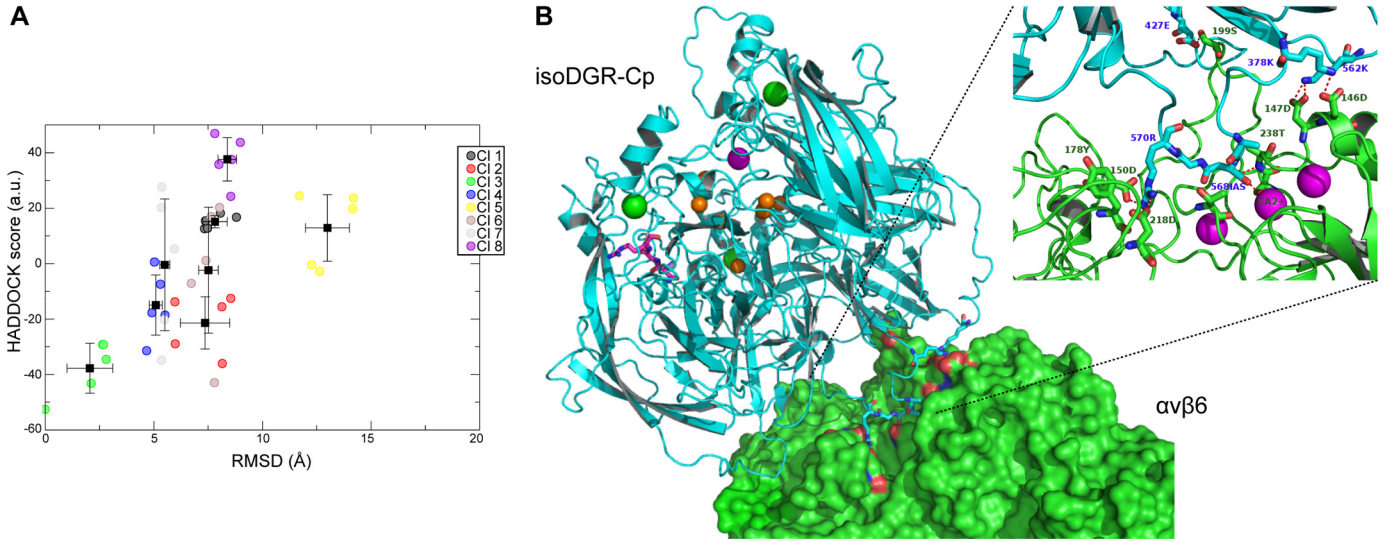

FIGURE 4. **Molecular docking model of isoDGR-Cp/αvβ6 integrin binding site.** *A*, HADDOCK scores *versus* root mean square deviations from the lowest energy complex structure for docking run performed of Cp-αvβ6. Different clusters are shown (*circles*) represented in different colors. They were obtained fitting the models on the backbone of the αvβ6-binding site and then calculating the root mean square deviation values from the lowest energy solutions over the heavy atoms of the Cp protein. Structures belong to the same cluster if they differ by less than 2 Å in the pairwise root mean square deviation matrix. The HADDOCK score corresponds to the weighted sum of different energy terms (van der Waals, electrostatic, and restraint energies). Cluster 3 is the best solution that is represented in *B*. *B*, HADDOCK model of isoDGR-Cp/αvβ6 integrin binding site. Surface representation of αvβ6 binding pocket (*green*) in complex with isoDGR-Cp (*cyan cartoon*). The side chains of the residues forming stable interactions (as reported in text) are shown in *licorice*. *Orange spheres* correspond to Cu^{2+} ions; *magenta spheres* correspond to Ca^{2+} cation; *green spheres* correspond to Na^{+} ions. *Red dotted lines* denote the hydrogen bonds of the Cp with αv and β6 subunits. In *magenta licorice* is shown the ^{962}NGR motif. The arginine of ^{568}isoDGR predominantly interacts with Asp^{150} of αv domain, whereas the same arginine can transiently interact with Asp^{218}. The isoaspartyl residue of isoDGR interacts with Ca^{2+} MIDAS ion located in the β6 domain (see zoomed area). Other interactions between ^{568}isoDGR-Cp and αvβ6 have been highlighted; in particular we noticed a strong and stable network of salt bridges between Lys^{562} and Lys^{369} of isoDGR-Cp and Asp^{146} and Asp^{147} of β6 domain of αvβ6 integrin (interaction reported in text).

Cp to bind αvβ6 integrin. However, the experimental evidence reported in Fig. 2 suggests that the deamidation of ^{962}NGR in oxidative conditions causes a considerable structural rearrangement that cannot be predicted by computational methods. Thus, we decided to perform molecular dynamics simulation only on ^{568}isoDGR-Cp protein to generate a set of reliable structures to be docked onto αvβ6.

Cluster analysis on the ^{568}isoDGR-Cp molecular dynamics allowed extraction of a number of representative structures of the simulations. A bundle of 27 isoDGR structures, corresponding to the center of the clusters, were docked onto a bundle of 10 αvβ6 structures, which are the center of the clusters obtained from 10 ns of molecular dynamics of the free αvβ6. To restrict the number of possible docked solutions, we defined a set of restrains (Cp-isoAsp^{568}: αvβ6-Asp^{150}, Asp^{218}, Ala^{143}, Pro^{184}, Phe^{185}, Thr^{238}; Cp-Gly^{569}: αvβ6-Asp^{150}, Asp^{218}, Ala^{143}, Pro^{184}, Phe^{185}, Thr^{238}; and Cp-Arg^{570}: αvβ6-Asp^{150}, Asp^{218}, Ala^{143}, Pro^{184}, Phe^{185}, Thr^{238}) corresponding to canonical RGD or isoDGR integrin-binding site (11) as suggested from competition experiments. The docking calculations led to different solutions (Fig. 4*A*) whereby the cluster 3, representing the best solution, showed that the ^{568}isoDGR-Cp docked onto αvβ6 integrin recapitulates the classical RGD/isoDGR receptor interactions (11) and creates some additional interactions (αvβ6/Cp: Ser^{199} β6/Glu^{427}, 1.7 ± 0.1 Å; Tyr^{178} αv/Arg^{570}, 2.1 ± 0.1 Å; Asp^{146} β6/Lys^{378}, 1.9 ± 0.3 Å; Thr^{238} β6/^{568}IAS, 1.9 ± 0.2 Å; Asp^{150} αv/Arg^{570}, 1.8 ± 0.2 Å; Asp^{147} β6/Lys^{562}, 1.9 ± 0.3 Å) (Fig. 4*B*).

Deamidated Cp Mediates Cellular Adhesion and Spreading—The binding to integrins observed *in vitro* might not reflect the real binding properties of deamidated Cp, given the possibility that adsorption of purified integrins on microtiter plates might alter their conformation. Furthermore, we have previously shown that the isoDGR site of fibronectin but not its corresponding NGR site can promote cell adhesion (10–12, 14). To assess whether Cp can generate an isoDGR motif able to recognize integrins in physiological conformations, we analyzed the effect of Cp aged under oxidative conditions on the adhesion of human epithelial (HaCaT), endothelial (E.A.hy926), and glioblastoma (T98G) cell lines. Preliminary flow cytometry analysis showed $\alpha v\beta 6$ expression by HaCaT, $\alpha v\beta 3$ and $\alpha v\beta 5$ expression by EA.hy926, and $\alpha v\beta 8$ expression by TG98 (data not shown).

Plates coated with ox/AmBic-Cp increased in a dose-dependent manner the adhesion and spreading of HaCaT cells, whereas untreated Cp induced little cell adhesion (Fig. 5*A* and *B*). In HaCat cells adhering to ox/ambic-Cp coated plates, cell spreading showed a significant ($p = 0.0087$) area increase (~20%) as compared with cells adhering to Cp coated plates (Fig. 5*C*). Similar pro-adhesive effects were observed with glioblastoma (Fig. 5*D* and *E*) and endothelial cell lines (data not shown).

To assess whether cell adhesion was mediated by isoDGR, we incubated ox/AmBic-treated Cp with PIMT, an enzyme that converts L-isoAsp residues to L-Asp (10, 30). PIMT treatment almost completely inhibited the pro-adhesive activity of ox/AmBic-treated Cp and of isoDGR peptide, the latter serving as a control (Student's *t* test, $p < 0.0001$) (Fig. 5*D* and *E*). These results suggest that isoAsp formation, presumably at NGR site(s) of Cp, is associated with a "gain of function" in cell adhesion assays.

Cp Aged under Oxidative Conditions Transduces Intracellular Signal through Integrin Engagement—Having observed that Cp after accelerated Asn aging under oxidative conditions was able to bind integrins expressed on the cell surface, we investigated whether this binding could also induce intracellular signaling. Signal transduction pathway analysis, as performed by reverse phase protein arrays on epithelial cells, indicated that cell incubation with ox/AmBic-treated Cp can induce coordinated phosphorylation events that recapitulate many of the steps of classical integrin-mediated signal transduction. Hierarchical clustering analysis of the comparison of treatment with either ox/AmBic-Cp or untreated Cp revealed that after 30 min: (*a*) there was an increase in the phosphorylation of the activation residues of several molecules, *e.g.*, p-Tyr^{397}FAK1, p-Thr^{514}PKCγ, p-Ser$^{217/221}$MEK1, p-Thr$^{185/202}$Tyr^{204}ERK1/2, p-Ser^{241}PDK1, p-Ser^{473}Akt, and (*b*) the phosphorylation of inhibitory residues, *e.g.*, p-Ser$^{9/21}$GSK3β, which in turn maintain β-catenin activity by preventing its phosphorylation (Fig. 6*A* and *B*). Several other proteins were unaffected (such as CrKl, SAPK/JNK, c-Jun, and Raf1) or slightly inhibited (PTEN and PKCα) (Fig. 6*A* and *B*). These results suggest that early signals mediated by deamidated Cp mostly addressed gene activation regulation, cell cycle, and MAPK signaling pathway (Fig. 7). In contrast, late signals (*i.e.*, immediately after 120 min of treatment) seemed to sustain actin cytoskeleton rearrangement rather than cell survival, proliferation, and MAPK pathway activation (Fig. 7). Src and CrkL were activated, and the phosphorylation of FAK1 was inhibited, concomitantly with the slight phosphorylation of PTEN and Raf1 inhibitory molecules, which block MEK1 and ERK1/2 activation (Fig. 6*A* and *B*; Fig. 7). Similarly, Akt inactivation results in β-catenin inhibition by Ser$^{33/37/45}$Thr^{41} phosphorylation, as mediated by GSK3β activation (Fig. 6*A* and *B*; Fig. 7).

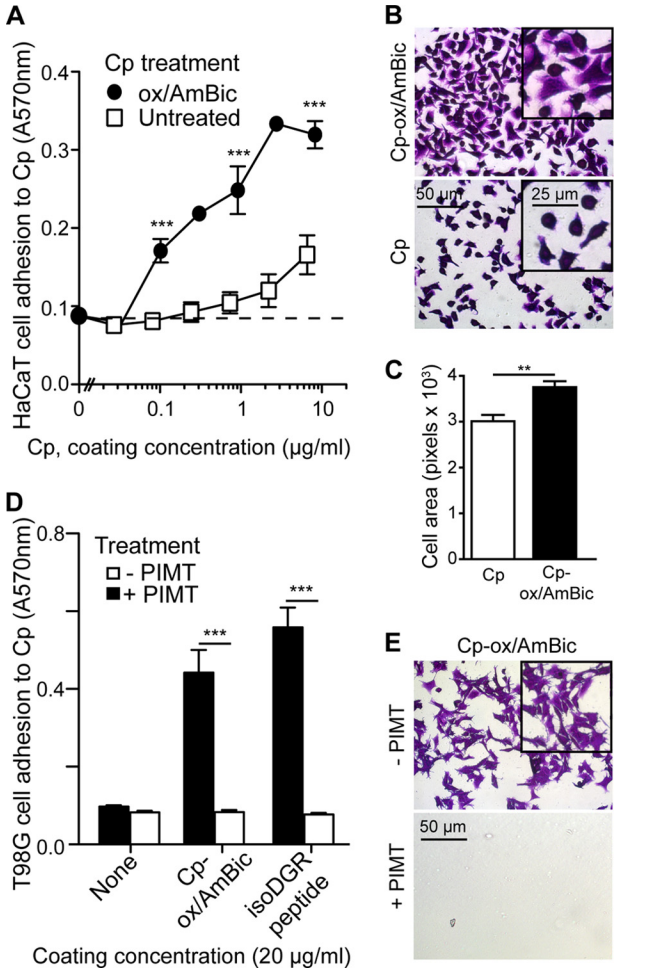

FIGURE 5. **Cp deamidation mediate cells adhesion and spreading via isoDGR/integrin interaction.** *A*, adhesion of epithelial HaCat cells to plates coated with different concentrations of either Cp (*Untreated*) or aged/oxidized Cp (*ox/AmBic*). Adhesion was evaluated as adsorbance at 570 nm of the crystal violet-stained cells. *B*, microscopy images of stained cells adherent to Cp-ox/AmBic, untreated Cp. Cell spreading is visible at higher magnification showed in the *boxes*. *C*, cell spreading was evaluated based on the pixel area automatically detected by image software analysis. Statistical significance was evaluated on cells measurement in three different microscopy fields for each condition (Cp, $n = 112$; Cp-ox/AmBic $n = 208$). **, $p = 0.0087$. *D*, adhesion of glioblastoma T98G cells to plastic coated either with BSA (*None*), aged/oxidized Cp (*ox/AmBic*), or the isoDGR peptide. Inhibition of cells adhesion occurred after treatment of coating proteins with PIMT (+) compared with the untreated wells (−). *E*, microscopy images of stained cells adherent to ox/AmBic-Cp treated with (+) or without (−) PIMT enzyme. All the adhesion assays were performed in triplicate for three independent experiments ($n = 3$). Statistical significance reported as *p* values was evaluated by Student's *t* test. ***, $p < 0.0001$.

Pathological CSF from Alzheimer Disease Fosters Integrin Binding of Spiked Purified Cp and Inhibits Its Ferroxidase Activity—To investigate whether Cp deamidation might occur also *in vivo*, in particular in pro-oxidant pathological CSF environments, we added purified Cp to CSF from healthy subjects or CSF from AD patients and incubated the mixture for 0, 3, 6,

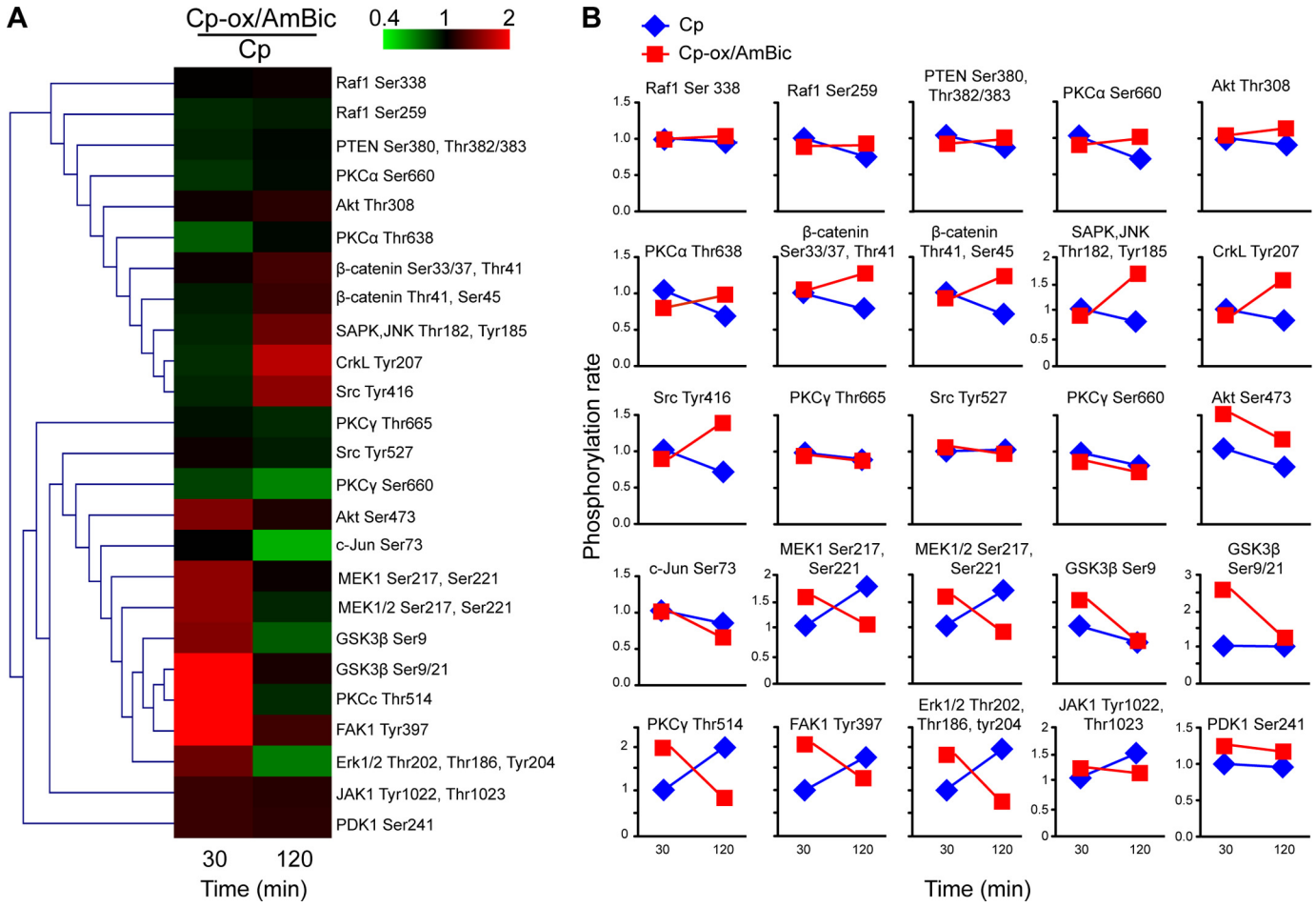

FIGURE 6. **Phosphorylation rate analysis of proteins belonging to the integrins signaling pathway as consequence of epithelial cells treatment with aged/oxidized Cp.** *A*, hierarchical clustering analysis of the reactivity of specific antibodies assessed by reverse phase protein arrays; the *columns* represent the rate of ox/AmBic-Cp *versus* Cp at two different treatment time ((Cp-ox/AmBic)/Cp 30 and 120 min), whereas the *rows* represent individual protein residue phosphorylation; the up- and down-regulated residue phosphorylation rate are respectively indicated in *red* and *green*. The intensity of color increases as the rate differences increase, as shown in the *bar*. *B*, expression profiles of clustered proteins. The *y* axes indicate the phosphorylation rate of the specific residue(s) as normalized with the total protein expression and compared with the phosphorylation level of control conditions (Cp) at 30 min of treatment; the *x* axes indicate the two different time (30 and 120 min) of Cp (*blue*) and ox/AmBic-Cp (*red*) treatments.

9, and 12 days at 37 °C. Cp was added in large amounts because of the presence of other integrin-binding molecules in CSF (*e.g.*, fibronectin, tenascin) that can compete the binding of Cp. Aging in a pathological milieu was able to induce a time-dependent Cp significant binding to $\alpha v\beta 6$ ($p < 0.0001$) (Fig. 8*A*, CSF/AD), whereas binding was absent or very weak when aging occurred in normal CSF (Fig. 8*A*, CSF). Thus, Cp deamidation showed a faster kinetic in the CSF from AD patients than from healthy subjects. By comparison with the binding ability of the same amount of *in vitro* chemically aged Cp (Cp-ox/AmBic), we ascertained that ~40% of the added Cp was converted to pro-adhesive Cp after 12 days of aging in AD patients CSF (Fig. 8*B*). Also in the case of purified Cp aging in the CSF, the gain in integrin binding properties was mediated by Cp deamidated NGR motifs, as demonstrated by competition with an isoDGR peptide, which abolished binding to $\alpha v\beta 6$ ($p = 0.0004$) (Fig. 8*C*, *gray bars*). To investigate whether Cp aged in pathological conditions was also able to recognize integrins in their physiological conformation, we performed cell adhesion experiments. HaCat cells were seeded on plates coated with Cp immunoprecipitated from either AD CSF or control CSF at time 0 or after 9 days of aging. The Cp aged in pathological CSF was able to promote the HaCat cell adhesion (Fig. 8*D*, *black bars*), whereas little or no adhesion was observed on Cp aged in control CSF (Fig. 8*D*, *white bars*). In addition to the acquisition of integrin binding function, Cp aged in AD CSF showed a complete loss of ferroxidase activity ($p < 0.0001$), whereas the Cp aged in healthy CSF showed a reduction of ~40% (Fig. 8*E*, 9 days).

DISCUSSION

Asparagine deamidation during protein aging depends on neighboring residues as well as on secondary and tertiary structural elements. The Asn deamidation rate is also affected by environmental factors such as pH, temperature, and ionic strength (1, 2). The combination of these features controls the kinetic of deamidation reactions that can range from hours to years (1, 2). Thus, for each protein it is important to assess whether specific Asn residues can undergo or not this post-translational modification. For example, we previously reported that the deamidation of an NGR site of fibronectin does not occur in the intact protein, whereas it can rapidly occur in protein fragments (10). The results reported here show that deamidation of

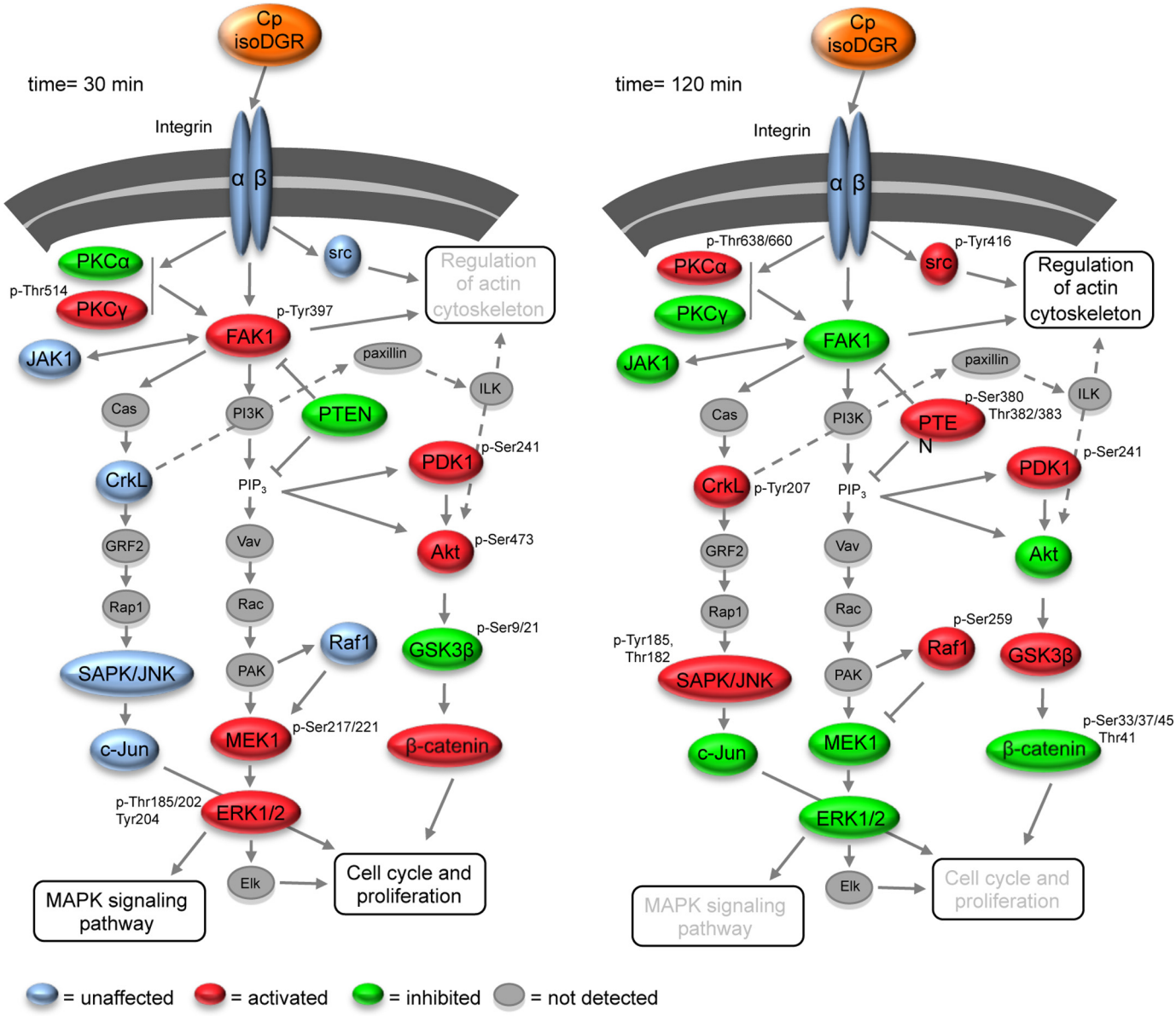

FIGURE 7. **Schematic representation of the signaling transduction throughout integrin engagement by Cp aged under oxidative conditions.** Changes in molecule phosphorylation after 30 and 120 min of treatment with deamidated Cp suggest that early signal is addressed to gene activation, cell cycle induction, and MAPK signaling pathway activation, whereas late signal sustains actin cytoskeleton rearrangement, and cell cycle and proliferation arrest. The schematic evaluation is based on the results obtained by activation signal analysis performed with reverse phase protein arrays (Fig. 6) and reports the rate of phosphorylation compared with control conditions consisting in cells treated with nonmodified Cp.

the ^{568}NGR site, which is exposed on the protein surface, does not require structural changes. In contrast, deamidation of the ^{962}NGR site, which is buried inside two β-strands of the protein structure and is blocked in a stable conformation by polar interactions with neighboring amino acids, can occur only after structural changes induced by an oxidative microenvironment. Protein oxidation and conformational changes similar to those reported here have been shown to cause copper ions to release from Cp (17, 26, 28). Noticeable, copper ions are necessary for the Cp ferroxidase activity (17, 26, 28). Because protein aging under oxidative stress is a condition that may occur in some neurodegenerative diseases (19, 31–33), we hypothesize that Cp aging under pathological conditions promotes modifications that favor structural changes that in turn foster both copper ion release and NGR deamidation. Copper ions released from Cp might contribute to the reported increase of the pool of free copper and to the decrease of active Cp found in the CSF of AD patients (34–36). It is conceivable that this increase, affecting the redox environment (37), might contribute to the observed Cp modifications by a feedback mechanism. The observed loss of ferroxidase activity of Cp aged in AD CSF suggests that changes in the Cp structure can be fostered also *ex vivo*. Given the role of Cp, ferroxidase activity reduction may affect the iron homeostasis (38), causing an increase in iron retention as seen in (17, 26, 28).

A relationship between oxidation and protein deamidation in neurodegenerative disease is also suggested by the observation that several proteins found to be deamidated in the brain of PIMT knock-out mouse were oxidized in the brain of AD patients (30). We previously reported that in the CSF from Par-

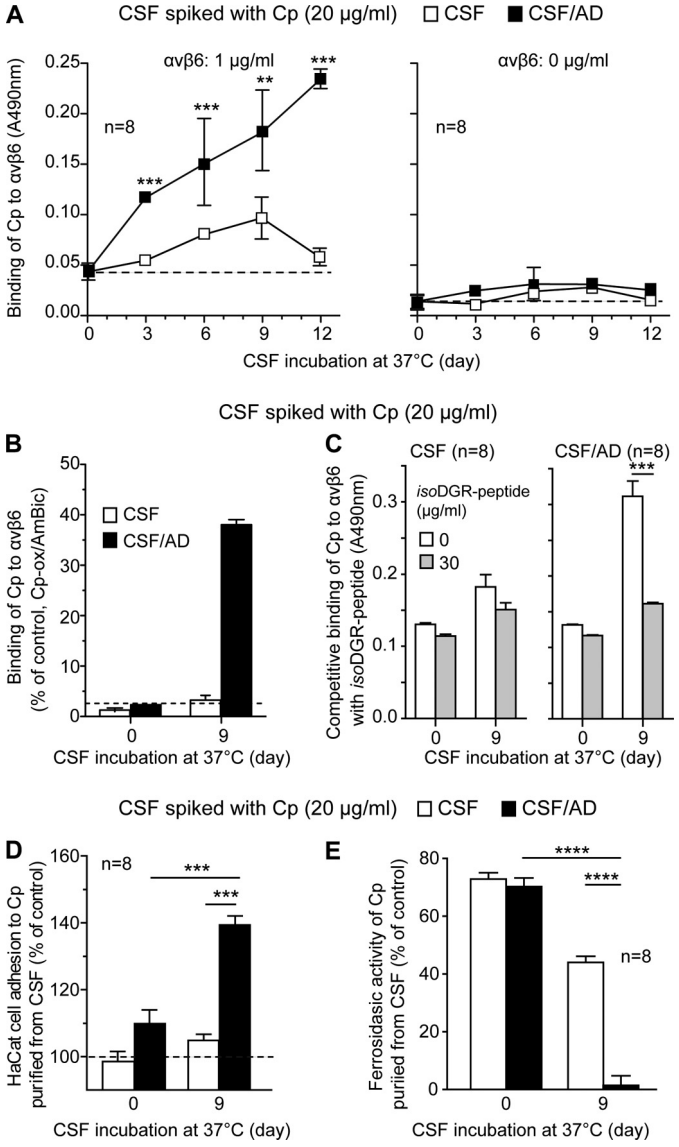

FIGURE 8. **Cerebrospinal fluid from Alzheimer disease patients fosters NGR motif deamidation and binding to αvβ6 integrin of spiked purified Cp.** *A*, binding to αvβ6 of purified Cp added to CSF from healthy subjects (*CSF*, *white squares*) or AD patients (*CSF/AD*, *black squares*) aged for 0, 3, 6, 9, and 12 days at 37 °C. *B*, quantitation of the Cp bound to αvβ6 integrin after *ex vivo* aging in CSF evaluated by the comparison with binding of chemically *in vitro* aged Cp (Cp-ox/AmBic, 100%). Aging from 0 to 9 days at 37 °C of purified Cp in the CSF from AD patients (*CSF/AD*) showed ~40% of the protein binding ability to αvβ6, whereas the same aging conditions in the CSF from healthy subjects showed negligible binding ability (3–4%). *C*, competition with isoDGR peptide (*gray bars*) of the binding to αvβ6 of Cp aged in CSF from healthy subjects or AD patients (CSF and CSF/AD, respectively, *white bars*). *D*, HaCat cell adhesion to plates coated with immunoprecipitated purified Cp (5 μg/ml) after *ex vivo* aging (0 or 9 days) in CSF from healthy subjects (*CSF*, *white bars*) or AD patients (*CSF/AD*, *black bars*). Adhesion was evaluated as absorbance (570 nm) of the crystal violet-stained cells and was expressed as a percentage of control (cells in adhesion on BSA-coated wells). *E*, Cp ferroxidase activity after incubation in CSF from healthy subjects (*CSF*, *white bars*) or AD patients (*CSF/AD*, *black bars*). Ferroxidase activity of immunoprecipitated Cp (1.25 μg) was evaluated measuring the decrease in Btp-Fe^{2+} complex absorbance at 535 nm. The values are expressed as percentages of total ferroxidase activity measured for 1.25 μg of untreated Cp. All the assays were performed in triplicate for two independent experiments, by using CSF from $n = 8$ different subjects each group (Table 1). Statistical *p* value was evaluated by Student's *t* test. ****, $p < 0.0001$; ***, $p < 0.001$; **, $p < 0.01$.

kinson disease and AD patients, Cp showed modifications derived from protein oxidation (17). Similar modifications have been reported for serum Cp during human aging (26). Thus, the Cp alterations observed in Parkinson disease and AD patients might reflect accelerated protein aging, as a consequence of changes in the environmental redox status of pathological CSF (18, 19). Therefore, it is plausible that the reported Cp oxidation-induced changes (17) also include Asn deamidation of NGR motifs.

Another major finding of this work is that the NGR to isoDGR conversion in Cp induces a gain of function in terms of binding to several αv integrins and, above all, the fact that the interaction of deamidated Cp with integrins can trigger an intracellular signaling cascade. We previously demonstrated that the NGR to isoDGR transition in fibronectin can work as a molecular switch for integrin-ligand recognition; the same mechanism seems to explain the gain of integrin binding function in Cp aged under oxidative conditions (10–12, 14). It is of relevance that, in contrast to fibronectin, the binding to integrin occurs for the intact full-length deamidated Cp. Consistently with binding data, our docking studies show that at least the ^{568}isoDGR motif of intact Cp can interact with the canonical RGD binding pocket of the αvβ6 having the stereochemical and electrostatic requirements for a correct recognition. Because it is not possible to predict *a priori* the putative structural rearrangement induced by the oxidation, we cannot describe *in silico* the possible interactions occurring between integrin and the ^{962}isoDGR sequence in the context of full-length Cp. The capability of the intact deamidated Cp to bind integrins might explain the ability to promote integrin activation.

These findings suggest that the Cp deamidation can produce a biological relevant gain of function. The functional importance of the NGR sites of Cp is also suggested by the high conservation of these tripeptide sequences across differing species from hamster to human. Remarkably, very few substitutions in various species were also shown in the ^{962}NGR flanking sequences, which are likely crucial for regulating the deamidation rate.

Notably, Cp NGR deamidation might occur in a relevant manner in certain pathological conditions, as suggested by the observation that Cp *ex vivo* aged in the CSF from AD patients acquires integrin binding and cell adhesion properties. The faster kinetic of Cp deamidation observed in CSF from AD patients compared with the CSF from healthy subjects supports the hypothesis of a generally accelerated protein aging in neurodegenerative diseases, as a consequence of pathological environment (18, 19). Based on the observation that after 12 days of aging in the pathological CSF ~40% of the Cp were able to bind integrin and given that the Cp concentration in the CSF is ~2 μg/ml and that its physiological half-life is ~5.5 days *in vivo* (15), it is conceivable that NGR deamidation might occur in patients to an extent that yields functionally relevant concentration of deamidated Cp (~200 ng/ml). The observed induction of NGR modification in Cp incubated in the CSF from AD patients implies the presence of factors that foster/accelerate deamidation, either directly or indirectly as a consequence of the induction of structural changes. However, further studies are necessary to define the differential composition of healthy and AD CSFs as to identify factors underlying the increased deamidation rate observed in pathological CSF.

It is known that integrin binding may activate intracellular signaling cascades, which in turn can affect cell differentiation, survival, growth, and division (39). Thereby, the hypothesis that in neurodegenerative diseases Cp might deamidate and transduce unusual intracellular signals opens new investigation perspectives in the AD field. It has been reported that an aberrant signaling mediated via integrin engagement (*e.g.*, $\alpha V\beta 1$, $\alpha 2\beta 1$, $\alpha V\beta 3$, and $\alpha V\beta 5$) by fibrillar amyloid-β in the CNS can result in unconventional FAK activation and downstream signaling (*i.e.*, MAPK, GSKβ3, etc.) (40–42). A similar signaling mechanism is triggered by deamidated Cp in epithelial cells: we observed inhibition of FAK and MAPK signaling, which could lead to cell cycle arrest, proliferation inhibition, and cytoskeleton reorganization. Various cell types in the CNS might be activated via integrins, including microglial cells, which contribute to the inflammation mechanisms in neurodegenerative diseases (43). Interestingly, it has been reported that Cp can activate microglial cells (44), although the receptor underlying this mechanism has not yet been identified: one possibility is that deamidated Cp interacts with integrins. Other potential cell targets of deamidated Cp include the specialized epithelial cells of the ependymal layer and choroid plexus, which are directly in contact with the CSF and have been reported to be altered in AD (45–47).

In conclusion, the results show that Asn deamidation reactions, which may occur in Cp upon aging, can convert this protein into an isoDGR-containing ligand of αv integrins. Furthermore, integrin-mediated intracellular signaling can be transduced by the modified protein. Oxidation-induced structural changes foster the NGR to isoDGR transition at the NGR site buried in the protein structure. Even though the mechanism we described results mainly from *in vitro* observations, the *ex vivo* evidence that the CSF from AD patients promotes Cp deamidation suggests that Cp modifications might also occur in patients. Further investigations are needed to assess the biological role of *in vivo* Cp deamidation and the consequences for neurodegenerative diseases.

REFERENCES

1. Weintraub, S. J., and Deverman, B. E. (2007) Chronoregulation by asparagine deamidation. *Sci. STKE* **2007,** re7
2. Robinson, N. E., Robinson, Z. W., Robinson, B. R., Robinson, A. L., Robinson, J. A., Robinson, M. L., and Robinson, A. B. (2004) Structure-dependent nonenzymatic deamidation of glutaminyl and asparaginyl pentapeptides. *J. Pept. Res.* **63,** 426–436
3. Robinson, N. E., and Robinson, A. B. (2001) Molecular clocks. *Proc. Natl. Acad. Sci. U.S.A.* **98,** 944–949
4. Ingrosso, D., D'Angelo, S., di Carlo, E., Perna, A. F., Zappia, V., and Galletti, P. (2000) Increased methyl esterification of altered aspartyl residues in erythrocyte membrane proteins in response to oxidative stress. *Eur. J. Biochem.* **267,** 4397–4405
5. Ingrosso, D., Cimmino, A., D'Angelo, S., Alfinito, F., Zappia, V., and Galletti, P. (2002) Protein methylation as a marker of aspartate damage in glucose-6-phosphate dehydrogenase-deficient erythrocytes. Role of oxidative stress. *Eur. J. Biochem.* **269,** 2032–2039
6. Watanabe, A., Takio, K., and Ihara, Y. (1999) Deamidation and isoaspartate formation in smeared tau in paired helical filaments. Unusual properties of the microtubule-binding domain of tau. *J. Biol. Chem.* **274,** 7368–7378
7. Shimizu, T., Matsuoka, Y., and Shirasawa, T. (2005) Biological significance of isoaspartate and its repair system. *Biol. Pharm. Bull.* **28,** 1590–1596
8. Hasegawa, M., Morishima-Kawashima, M., Takio, K., Suzuki, M., Titani, K., and Ihara, Y. (1992) Protein sequence and mass spectrometric analyses of Tau in the Alzheimer's disease brain. *J. Biol. Chem.* **267,** 17047–17054
9. Shimizu, T., Watanabe, A., Ogawara, M., Mori, H., and Shirasawa, T. (2000) Isoaspartate formation and neurodegeneration in Alzheimer's disease. *Arch. Biochem. Biophys.* **381,** 225–234
10. Curnis, F., Longhi, R., Crippa, L., Cattaneo, A., Dondossola, E., Bachi, A., and Corti, A. (2006) Spontaneous formation of L-isoaspartate and gain of function in fibronectin. *J. Biol. Chem.* **281,** 36466–36476
11. Spitaleri, A., Mari, S., Curnis, F., Traversari, C., Longhi, R., Bordignon, C., Corti, A., Rizzardi, G. P., and Musco, G. (2008) Structural basis for the interaction of isoDGR with the RGD-binding site of $\alpha v\beta 3$ integrin. *J. Biol. Chem.* **283,** 19757–19768
12. Curnis, F., Cattaneo, A., Longhi, R., Sacchi, A., Gasparri, A. M., Pastorino, F., Di Matteo, P., Traversari, C., Bachi, A., Ponzoni, M., Rizzardi, G. P., and Corti, A. (2010) Critical role of flanking residues in NGR-to-isoDGR transition and CD13/integrin receptor switching. *J. Biol. Chem.* **285,** 9114–9123
13. Frank, A. O., Otto, E., Mas-Moruno, C., Schiller, H. B., Marinelli, L., Cosconati, S., Bochen, A., Vossmeyer, D., Zahn, G., Stragies, R., Novellino, E., and Kessler, H. (2010) Conformational control of integrin-subtype selectivity in isoDGR peptide motifs. A biological switch. *Angew. Chem. Int. Ed. Engl.* **49,** 9278–9281
14. Corti, A., and Curnis, F. (2011) Isoaspartate-dependent molecular switches for integrin-ligand recognition. *J. Cell Sci.* **124,** 515–522
15. Hellman, N. E., and Gitlin, J. D. (2002) Ceruloplasmin metabolism and function. *Annu. Rev. Nutr.* **22,** 439–458
16. Vashchenko, G., and MacGillivray, R. T. (2013) Multi-copper oxidases and human iron metabolism. *Nutrients* **5,** 2289–2313
17. Olivieri, S., Conti, A., Iannaccone, S., Cannistraci, C. V., Campanella, A., Barbariga, M., Codazzi, F., Pelizzoni, I., Magnani, G., Pesca, M., Franciotta, D., Cappa, S. F., and Alessio, M. (2011) Ceruloplasmin oxidation, a feature of Parkinson's disease CSF, inhibits ferroxidase activity and promotes cellular iron retention. *J. Neurosci.* **31,** 18568–18577
18. Grimm, S., Hoehn, A., Davies, K. J., and Grune, T. (2011) Protein oxidative modifications in the ageing brain. Consequence for the onset of neurodegenerative disease. *Free Radic. Res.* **45,** 73–88
19. Zecca, L., Youdim, M. B., Riederer, P., Connor, J. R., and Crichton, R. R. (2004) Iron, brain ageing and neurodegenerative disorders. *Nat. Rev. Neurosci.* **5,** 863–873
20. McKhann, G., Drachman, D., Folstein, M., Katzman, R., Price, D., and Stadlan, E. M. (1984) Clinical diagnosis of Alzheimer's disease. Report of the NINCDS-ADRDA Work Group under the auspices of Department of Health and Human Services Task Force on Alzheimer's Disease. *Neurology* **34,** 939–944
21. Zhang, Y. (2008) I-TASSER server for protein 3D structure prediction. *BMC Bioinformatics* **9,** 40
22. Hess, B., Kutzner, C., van der Spoel, D., and Lindahl, E. (2008) GROMACS 4. Algorithms for highly efficient, load-balanced, and scalable molecular simulation. *J. Chem. Theory Comput.* **4,** 435–447
23. de Vries, S. J., van Dijk, A. D., Krzeminski, M., van Dijk, M., Thureau, A., Hsu, V., Wassenaar, T., and Bonvin, A. M. (2007) HADDOCK versus HADDOCK. New features and performance of HADDOCK2.0 on the CAPRI targets. *Proteins* **69,** 726–733
24. Saeed, A. I., Sharov, V., White, J., Li, J., Liang, W., Bhagabati, N., Braisted, J., Klapa, M., Currier, T., Thiagarajan, M., Sturn, A., Snuffin, M., Rezantsev, A., Popov, D., Ryltsov, A., Kostukovich, E., Borisovsky, I., Liu, Z., Vinsavich, A., Trush, V., and Quackenbush, J. (2003) TM4. A free, open-source system for microarray data management and analysis. *BioTechniques* **34,** 374–378
25. Bento, I., Peixoto, C., Zaitsev, V. N., and Lindley, P. F. (2007) Ceruloplasmin revisited. Structural and functional roles of various metal cation-binding sites. *Acta Crystallogr. D Biol. Crystallogr.* **63,** 240–248
26. Musci, G., Bonaccorsi di Patti, M. C., Fagiolo, U., and Calabrese, L. (1993) Age-related changes in human ceruloplasmin. Evidence for oxidative modifications. *J. Biol. Chem.* **268,** 13388–13395
27. Kang, J. H., Kim, K. S., Choi, S. Y., Kwon, H. Y., and Won, M. H. (2001) Oxidative modification of human ceruloplasmin by peroxyl radicals.

Biochim. Biophys. Acta **1568,** 30–36
28. Sedlák, E., Zoldák, G., and Wittung-Stafshede, P. (2008) Role of copper in thermal stability of human ceruloplasmin. *Biophys. J.* **94,** 1384–1391
29. Dehart, M. P., and Anderson, B. D. (2012) A mechanism-based kinetic analysis of succinimide-mediated deamidation, racemization, and covalent adduct formation in a model peptide in amorphous lyophiles. *J. Pharm. Sci.* **101,** 3096–3109
30. Zhu, J. X., Doyle, H. A., Mamula, M. J., and Aswad, D. W. (2006) Protein repair in the brain, proteomic analysis of endogenous substrates for protein L-isoaspartyl methyltransferase in mouse brain. *J. Biol. Chem.* **281,** 33802–33813
31. Texel, S. J., Xu, X., and Harris, Z. L. (2008) Ceruloplasmin in neurodegenerative diseases. *Biochem. Soc. Trans.* **36,** 1277–1281
32. Ayton, S., Lei, P., Duce, J. A., Wong, B. X., Sedjahtera, A., Adlard, P. A., Bush, A. I., and Finkelstein, D. I. (2013) Ceruloplasmin dysfunction and therapeutic potential for Parkinson disease. *Ann. Neurol.* **73,** 554–559
33. Dawson, T. M., and Dawson, V. L. (2003) Molecular pathways of neurodegeneration in Parkinson's disease. *Science* **302,** 819–822
34. Capo, C. R., Arciello, M., Squitti, R., Cassetta, E., Rossini, P. M., Calabrese, L., and Rossi, L. (2008) Features of ceruloplasmin in the cerebrospinal fluid of Alzheimer's disease patients. *Biometals* **21,** 367–372
35. Arnal, N., Cristalli, D. O., de Alaniz, M. J., and Marra, C. A. (2010) Clinical utility of copper, ceruloplasmin, and metallothionein plasma determinations in human neurodegenerative patients and their first-degree relatives. *Brain Res.* **1319,** 118–130
36. Brewer, G. J., Kanzer, S. H., Zimmerman, E. A., Celmins, D. F., Heckman, S. M., and Dick, R. (2010) Copper and ceruloplasmin abnormalities in Alzheimer's disease. *Am. J. Alzheimers Dis. Other Demen* **25,** 490–497
37. Eskici, G., and Axelsen, P. H. (2012) Copper and oxidative stress in the pathogenesis of Alzheimer's disease. *Biochemistry* **51,** 6289–6311
38. Patel, B. N., Dunn, R. J., Jeong, S. Y., Zhu, Q., Julien, J. P., and David, S. (2002) Ceruloplasmin regulates iron levels in the CNS and prevents free radical injury. *J. Neurosci.* **22,** 6578–6586
39. Luo, B. H., Carman, C. V., and Springer, T. A. (2007) Structural basis of integrin regulation and signaling. *Annu. Rev. Immunol.* **25,** 619–647
40. Grace, E. A., and Busciglio, J. (2003) Aberrant activation of focal adhesion proteins mediates fibrillar amyloid β-induced neuronal dystrophy. *J. Neurosci.* **23,** 493–502
41. Wright, S., Malinin, N. L., Powell, K. A., Yednock, T., Rydel, R. E., and Griswold-Prenner, I. (2007) $\alpha 2\beta 1$ and $\alpha V\beta 1$ integrin signaling pathways mediate amyloid-β-induced neurotoxicity. *Neurobiol. Aging* **28,** 226–237
42. Caltagarone, J., Jing, Z., and Bowser, R. (2007) Focal adhesions regulate Aβ signaling and cell death in Alzheimer's disease. *Biochim. Biophys. Acta* **1772,** 438–445
43. Glass, C. K., Saijo, K., Winner, B., Marchetto, M. C., and Gage, F. H. (2010) Mechanisms underlying inflammation in neurodegeneration. *Cell* **140,** 918–934
44. Lee, K. H., Yun, S. J., Nam, K. N., Gho, Y. S., and Lee, E. H. (2007) Activation of microglial cells by ceruloplasmin. *Brain Res.* **1171,** 1–8
45. Perez-Gracia, E., Blanco, R., Carmona, M., Carro, E., and Ferrer, I. (2009) Oxidative stress damage and oxidative stress responses in the choroid plexus in Alzheimer's disease. *Acta Neuropathol.* **118,** 497–504
46. Krzyzanowska, A., and Carro, E. (2012) Pathological alteration in the choroid plexus of Alzheimer's disease. Implication for new therapy approaches. *Front. Pharmacol.* **3,** 75
47. Serot, J. M., Zmudka, J., and Jouanny, P. (2012) A possible role for CSF turnover and choroid plexus in the pathogenesis of late onset Alzheimer disease. *J. Alzheimers Dis.* **30,** 17–26